The interaction of quasi-particles in graphene with chemical dopants

Aaron Bostwick[1]**, Taisuke Ohta**[2]**, Jessica L McChesney**[1]**,
Konstantin V Emtsev**[3]**, Florian Speck**[3]**, Thomas Seyller**[3]**,
Karsten Horn**[4]**, Stephan D Kevan**[5] **and Eli Rotenberg**[1,6]

[1] Advanced Light Source, E O Lawrence Berkeley National Laboratory,
Berkeley, CA 94720, USA
[2] Sandia National Laboratory, Surface and Interface Science Department,
Albuquerque, NM 87185, USA
[3] Lehrstuhl für Technische Physik, Universität Erlangen-Nürnberg,
91058 Erlangen, Germany
[4] Department of Molecular Physics, Fritz-Haber-Institut der
Max-Planck-Gesellschaft, 14195 Berlin, Germany
[5] Department of Physics, University of Oregon, Eugene, OR 97403, USA
E-mail: erotenberg@lbl.gov

Abstract. We review recent developments on the electronic properties of graphene under the influence of adsorbates. Potassium and hydrogen adsorbed on graphene induce very different effects on the graphene electron gas because of the different types—ionic versus covalent—of chemical bonds formed. Potassium readily donates electrons to graphene, and the resulting Fermi sea shows strong electron–plasmon scattering but weak defect scattering. In contrast, hydrogen adsorption saturates a carbon π bond, leading to the removal of electrons from the graphene. Such hydrogen bonds act as a lattice defect, leading to a sharp reduction in conductivity and an insulating temperature dependence of the resistivity. The marked contrast in the behaviour of these adsorbates derives from the different symmetry classes of their defect geometries.

[6] Author to whom any correspondence should be addressed.

IOP Institute of Physics ⚛ DEUTSCHE PHYSIKALISCHE GESELLSCHAFT

Contents

1. Introduction

The use of graphene in novel devices depends on a detailed understanding of its electronic properties as a function of doping and its behaviour in the presence of defects. These topics are also fundamentally interesting because of the unique properties of graphene that are derived from its novel electronic structure. Namely, the charge carriers in graphene are formally equivalent to massless Dirac fermions, carrying an extra pseudospin quantum number (in addition to the ordinary spin), which strongly impacts their interactions with each other and with defects [1]–[5].

In order to investigate these properties, we have systematically studied the electronic properties of graphene dopants using angle-resolved photoemission spectroscopy (ARPES) with *in situ* deposition of various chemical dopants [6]–[9]. In particular, hydrogen and potassium have been studied because of their different bonding configurations, which lead to either a predicted magnetic state [10] or (in the case of K-doped bulk graphite) a superconducting state [11]. These very different phenomena in ordered compounds ultimately derive from the different bonding geometries of the K or H atoms [12]–[14]. Similarly divergent behaviours can also be found for very low coverage adsorption of H or K atoms, as we will discuss [7, 9].

These differences are highlighted in figure 1, which shows the expected atomic arrangements around K and H atoms. The K atoms bond ionically to the graphene, donating their outer s-electron, and prefer to sit in the hollow site of the honeycomb carbon mesh [15]. At low density, the H atoms are expected to bond tetrahedrally to a single C atom, converting its local bonding arrangement from sp^2 to an sp^3 arrangement [16]. This is found experimentally to lead to p-doping of the graphene, since each H atom could be naively expected to remove a single C π electron from the electron gas in the graphene [9].

Graphene samples were fabricated with two recipes. In the first part of this paper, samples were grown by etching the (0001) surface of SiC wafers in H_2 gas, and then transferred through air to an ultra-high vacuum (UHV) chamber, where graphene layers were formed by surface decomposition at elevated temperature [17]–[19]. After this procedure, one finds two carbon layers at the surface, the '0th' or buffer layer at the interface and an active, *n*-doped graphene layer at the surface [18, 19]. In the second part of this paper, we used quasi-free-standing graphene, as discussed later.

ARPES was conducted on the samples in the same chamber as the final graphene preparation. Spectra were acquired using a Scienta SES-R4000 analyzer, from samples held at $T = 20$ K on a liquid-He-cooled goniometer capable of three independent sample rotations and three orthogonal spatial motions. Photoelectrons were generated using a 50 μm beam of soft x-rays (photon energy $h\nu = 95$ eV) generated at beamline 7.0 of the Advanced Light Source; total energy resolution (photon+electron) was less than 30 meV, and momentum resolution is estimated to be 0.01 Å^{-1}.
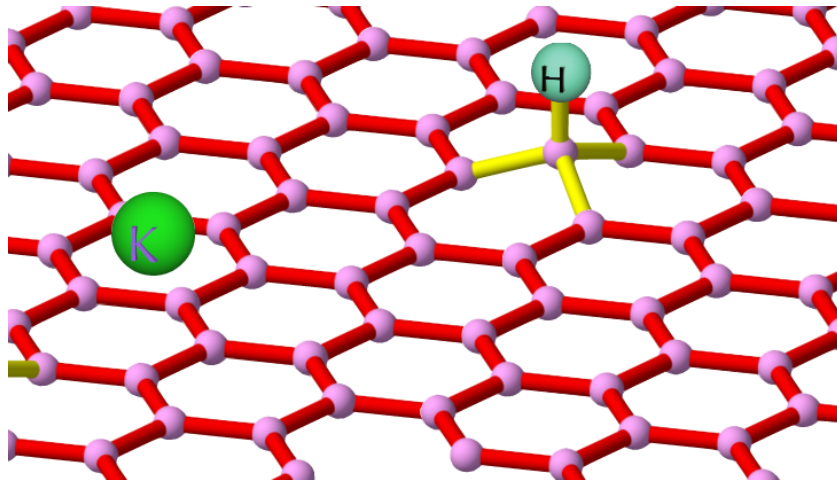
Figure 1. The expected bonding arrangements of K and H atoms adsorbed on graphene.

Samples were exposed to fluxes of atomic H or K at the same time that photoelectron spectra were measured. The atomic sources consisted of a heated tungsten capillary through which H_2 gas was passed (for atomic hydrogen) or a commercial getter source (SAES) for potassium. The base pressure of the chamber was better than 2×10^{-11} torr.

The ARPES measurement is useful, because it accesses the electronic self-energy function $\Sigma(\mathbf{k}, \omega)$ (this topic is reviewed in [20, 21]). This complex function describes, in its real part, the renormalization of the single-particle energy as a function of momentum $\mathbf{k}$ and electron binding energy ω. Since the electronic group velocity is $\partial\omega/\partial k$, any renormalization of the energy dispersion $\omega(k)$ amounts to a renormalization of the electron velocity. The imaginary part of $\Sigma(\mathbf{k}, \omega)$ describes the momentum- and binding-energy dependence of the lifetime due to scattering from other entities such as electrons, plasmons, electron–hole pairs or vibrations.

There is an exact analogy between the complex self-energy function Σ describing electron passage through a disordered medium and the complex index of refraction n that describes the propagation of photons through disordered dielectric media. In the latter, the real and complex parts of n describe the velocity renormalization and scattering of photons, respectively. Just as for the index of refraction, $\mathrm{Im}\,\Sigma(\mathbf{k}, \omega)$ and $\mathrm{Re}\,\Sigma(\mathbf{k}, \omega)$ are not independent, but mutually transform into each other through Hilbert (also known as Kramers–Kronig) transformation in order to preserve causality.

In the quasi-particle formulation of ARPES, the measured spectrum is equivalent to the single-particle spectral function

$$A(\mathbf{k}, \omega) = \frac{\pi^{-1}\,|\mathrm{Im}\,\Sigma(\mathbf{k}, \omega)|}{(\omega - \omega_b(\mathbf{k}) - \mathrm{Re}\,\Sigma(\mathbf{k}, \omega))^2 + (\mathrm{Im}\,\Sigma(\mathbf{k}, \omega))^2}, \tag{1}$$

a Lorentzian-like function whose position relative to the bare or unrenormalized band ω_b is given by $\mathrm{Re}\Sigma(\mathbf{k}, \omega)$ and whose width is given by $\mathrm{Im}\Sigma(\mathbf{k}, \omega)$. The function $A(\mathbf{k}, \omega)$ can be accessed in ARPES, where it is modulated by the Fermi–Dirac distribution (since we can observe only occupied states) and by optical matrix element effects that might restrict which bands may be observed. By the detection of the emitted photoelectron, we measure the lifetime of the remaining photohole left behind.
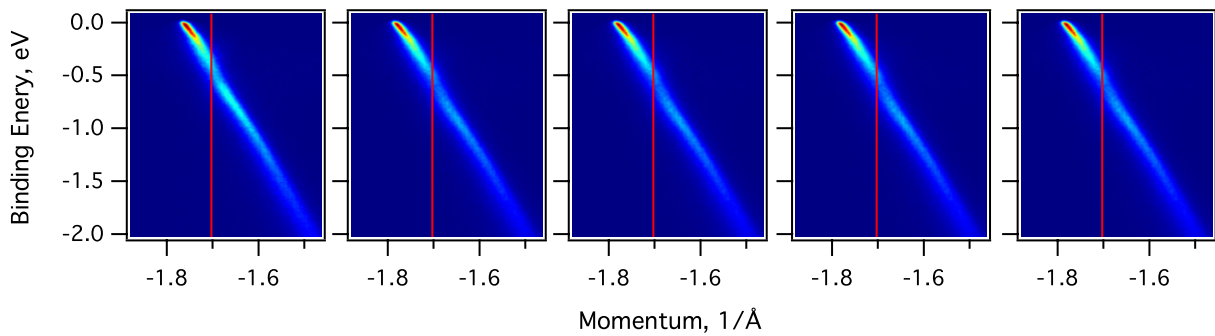
Figure 2. Variation of the band structure of graphene with potassium doping starting from (leftmost) pristine graphene and (rightmost) approximately 1% of a monolayer of K atoms. The vertical lines represent the corner (K) point of the graphene Brillouin zone (from [7]).

In the absence of interactions, $\Sigma \to 0$ and equation (1) reduces to a Dirac delta-function along the bare band $\omega = \omega_b(\mathbf{k})$. When the momentum dependence of the electron lifetime is weak, equation (1) reduces to a simple Lorentzian in the energy or momentum directions for each constant binding energy ω. Such a constant-energy slice of the spectral function is called a momentum-distribution curve (MDC) and, along the momentum axis, its width is simply the inverse mean free path of the charge carriers.

In this paper, we discuss the interpretation of the spectral function for graphene in the presence of K and H adsorbates. In section 2, we focus on the properties of K-doped graphene, in which equation (1) is validated. Two limits are explored, in which the k-dependence of $\Sigma(\mathbf{k}, \omega)$ is either weak or strong, depending on certain properties of the graphene–substrate interface. In section 3, we focus on the properties of H-doped graphene, where we show a complete breakdown of equation (1) due to the symmetry breaking induced by the H atoms.

2. Potassium on graphene

Figure 2 shows the evolution of the graphene spectral function $A(\mathbf{k}, \omega)$ starting from the pristine sample and for progressively higher doses of K atoms [7]. Rather than two crossed bands as expected from the graphene band structure, a single band is observed because one of the bands is extinguished by a vanishing photoemission matrix element [22]–[24]. As the surface is doped, the band shifts rigidly down to a good approximation, with a commensurate increase in the radius of the nearly circular Fermi surface. From the increased Fermi surface area, we can deduce the density of K atoms deposited, which is of the order of 1% of a monolayer for the doping range studied (assuming each K atom donates ∼1 electron). As the doping proceeds, a more or less linear band dispersion is maintained, with only moderate change in the shape of the dispersion related to the self-energy effects described above. In particular, we consider the MDC cut of the data at the Fermi energy E_F (where $\omega \to 0$) shown in figure 3(a). These data are fitted to Gaussian-broadened Lorentzians using a fixed Gaussian contribution of 0.01 Å^{-1} for each curve, representing the instrumental broadening.

From these fits we can derive some important quantities. From the peak positions, and the approximation that the Fermi surface is circular, we determine the charge density n at each
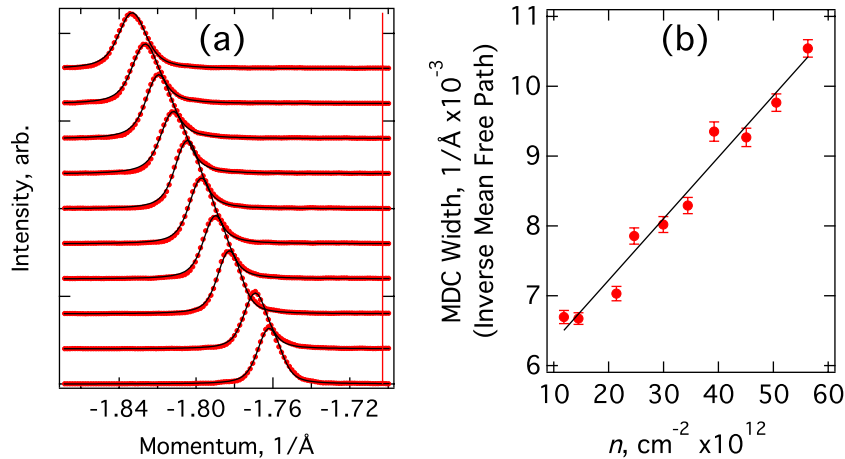
Figure 3. (a) The MDC at the Fermi level for K-doped graphene for various K dopings starting from clean- (bottom) to high-doping density $n = 5.6 \times 10^{13}\,\text{cm}^{-2}$ (top). (b) The fitted Lorentzian width, equivalent to the inverse mean-free path, extracted from each MDC curve as a function of the total charge density n.

doping stage. From the fact that a Lorentzian describes the MDC lineshapes well, we find that the k-dependence of the self-energy $\Sigma(\mathbf{k}, \omega)$ is negligible, at least near E_F. From the fitted widths Δk of these peaks, we accurately determine the inverse mean free path of the carriers at E_F, plotted in figure 3(b). In the clean samples, this measurement is nearly resolution-limited, but with potassium dosing, we observe a systematic increase in the linewidth, reflecting the scattering rate of the photohole from the K atoms.

The most important finding is that this scattering rate is relatively low, so that the observed momentum spread is much smaller than the Fermi wavelength k_F, i.e. the radius of the Fermi surface. This and the sharp linewidths of the bands in the energy direction indicate that the perturbations from scattering are weak and that the observed ARPES data in figure 1 are a good measure of the many-body interactions. Equivalently, we say that the quasi-particle picture is valid, since the quasi-particle lifetimes are long by these measures.

In light of the deviations of the observed band from the expected linear dispersion of graphene, we expect that certain kinks in the bands of figure 1 originate from a finite self-energy due to many-body interactions [7, 23]. These kinks can be observed in two places: first, at $\omega \sim 200\,\text{meV}$ below E_F; secondly, at the Dirac energy E_D where the band crosses at the K-point of the Brillouin zone (at $k = 1.703\,\text{\AA}^{-1}$).

To investigate the validity of this conclusion, it is necessary to find a complex self-energy $\Sigma(\mathbf{k}, \omega) = \text{Re}\,\Sigma(\mathbf{k}, \omega) + i\text{Im}\,\Sigma(\mathbf{k}, \omega)$, which when applied to equation (1) (using a linear bare band) can model both the kinks and the associated linewidths. Such a self-energy function must also be self-consistent (i.e. its real and imaginary parts must transform into each other) and, if successful, will provide a physical basis for interpreting the ARPES spectral function.

The momentum distributions in figure 3(a) are Lorentzian curves to a good approximation, which according to equation (1) should occur in general only for momentum-independent self-energy functions, i.e. $\Sigma(\mathbf{k}, \omega) \sim \Sigma(\omega)$. Within this assumption and assuming a linear bare band, we could extract the real and imaginary parts of the self-energy, which are shown in figure 4 for
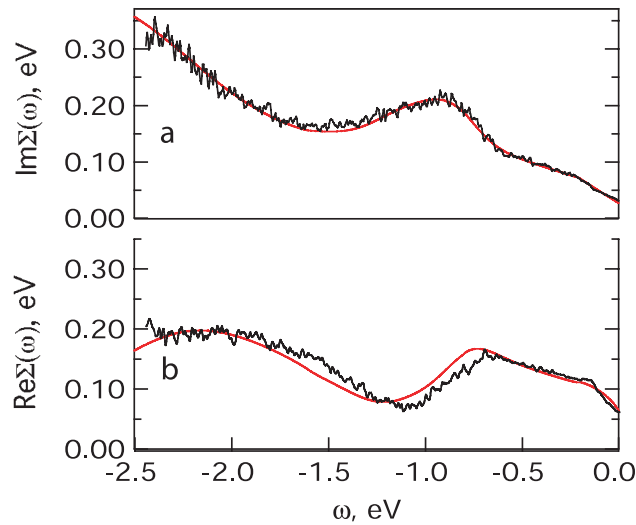
Figure 4. (a) Real and (b) imaginary parts (black) of the self-energy function $\Sigma(\mathbf{k}, \omega)$ extracted from ARPES data for K-doped graphene ($n = 5.6 \times 10^{13}$ cm^{-2}) assuming a linear bare band ω_b and neglecting any k-dependence. The red line in (a) is a smoothed version of the data; its Hilbert transform is shown as the red line in (b). Reproduced from [23] with permission from IOP Publishing.

highly doped K on graphene [23]. The extracted real part Re $\Sigma(\mathbf{k}, \omega)$ (black line in figure 4(b)) is found to be in good agreement with the inferred real part (red line in figure 4(b)) determined by the Hilbert transformation of the measured Im $\Sigma(\mathbf{k}, \omega)$. This provides strong evidence that equation (1) provides a self-consistent description of our data, with the self-energy extracted from the data, as shown in figure 4. Not only does this interpretation confirm that causality is preserved but also it excludes alternative interpretations of the data, such as a modification of the bare band structure due to symmetry breaking [25, 26].

Thus, the enhanced scattering rate above the phonon energy scale and near E_D could be considered to arise from purely energy-dependent processes. These processes were identified as originating from electron–phonon [7, 27, 28] and electron–plasmon scattering [7], [29–32], respectively.

However, in a finer analysis, the k-independent self-energy approximation can be seen to break down, especially at the highest doping, as illustrated in figure 5, which compares the MDC curves near E_F and E_D. This is established by an asymmetry in the MDC curve at E_D, suggesting a preferential scattering of states towards the K-point in the graphene valence band. The existence of asymmetry affects our analysis because analyzing the MDCs in terms of a Lorentzian lineshape will bias the peak positions and widths away from their actual values. This results, in all likelihood, in the residual deviation between direct and extracted Re $\Sigma(\mathbf{k}, \omega)$ shown in figure 4(b).

Such a momentum-dependent self-energy was predicted to arise from either the Coulomb interaction [29]–[32] or defect scattering [33, 34]. Although hints of these predicted self-energy functions can be seen in the data, sufficient details are not available in the photoemission results in order to discriminate between these and other models. In particular, some predictions based on the Coulomb interaction [29]–[31] predict a splitting of the main band into two bands, which might be consistent with the asymmetric lineshape in figure 5. However, the experimental splitting is much smaller than predictions.
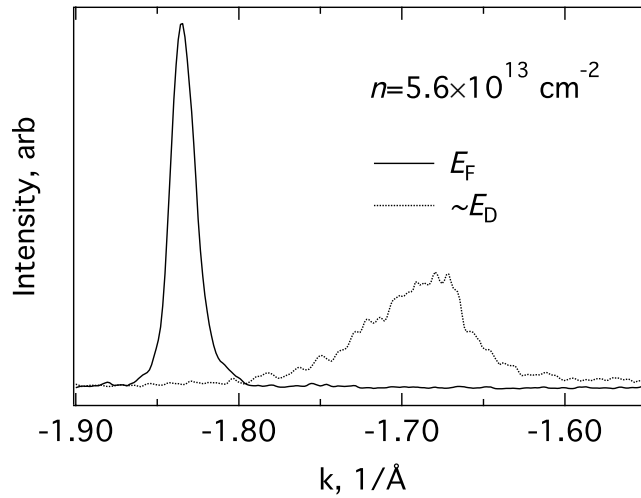
Figure 5. The MDC for highly K-doped graphene at E_F and just below E_D, at a binding energy of -0.9 eV for the indicated charge density.

A better understanding of the observed lineshapes could not be developed until the advent of quasi-free-standing graphene samples on SiC [35, 36]. In these samples, the graphene has been grown not on a dead carbon-rich buffer layer [19], but rather on top of a hydrogen-saturated SiC surface. For such a sample, the ARPES spectrum was taken in the same geometry and for a similar doping level as the upper doping limit of figure 2. Instead of a single quasi-particle band, we now clearly resolve a second band at greater binding energy (see figure 6(b)). Although the band is weak near E_F, it is quite strong near the Dirac crossing near the K-point. Here, the reconstruction of the spectral function from the ordinary graphene/SiC samples is most pronounced. As a result of the circular symmetry about the K-point, a cut of the bands along a perpendicular direction in k-space (figure 6(a)) shows that the Dirac crossing region, originally consisting of a single point, is now reconstructed into three crossings at energies E_{0-2}.

The momentum distribution cut at $E_F = 0.43$ eV (figure 6(c)) shows two circular contours associated with the two bands in figure 6(b); since these contours have the same crescent-like intensity profile about the K-point, we can conclude that at a given **k**, both bands have the same symmetry and therefore chiral pseudospin vector [22]–[24]. Similar considerations of all the observed features let us conclude that the band crossings at E_{0-2} are in fact Dirac crossings, always between states of opposite chirality.

A full account of the physical origin of this band splitting is provided elsewhere [29]–[31], [37] but can be briefly summarized as follows. Free charges in graphene interact through a screened Coulomb interaction. The screening is described by a momentum- and energy-dependent dielectric function, whose details can be calculated based on the linear dispersion of graphene's bands. From the dielectric function, one can calculate the excitation probability of electron–hole pairs (which are responsible for short-range screening of the Coulomb interaction) and plasmons (which dominate long-range Coulomb interaction) [38].

The existence of these two excitation pathways is responsible for the observation of two quasi-particles: the band of lower binding energy is an ordinary quasi-particle, whose lifetime is governed mainly by decay into electron–hole pairs and plasmons (as discussed previously [7]). The new band of higher binding energy is a quasi-particle described as an ordinary charge coupled strongly to a plasmon. This new quasi-particle can be thought of as a
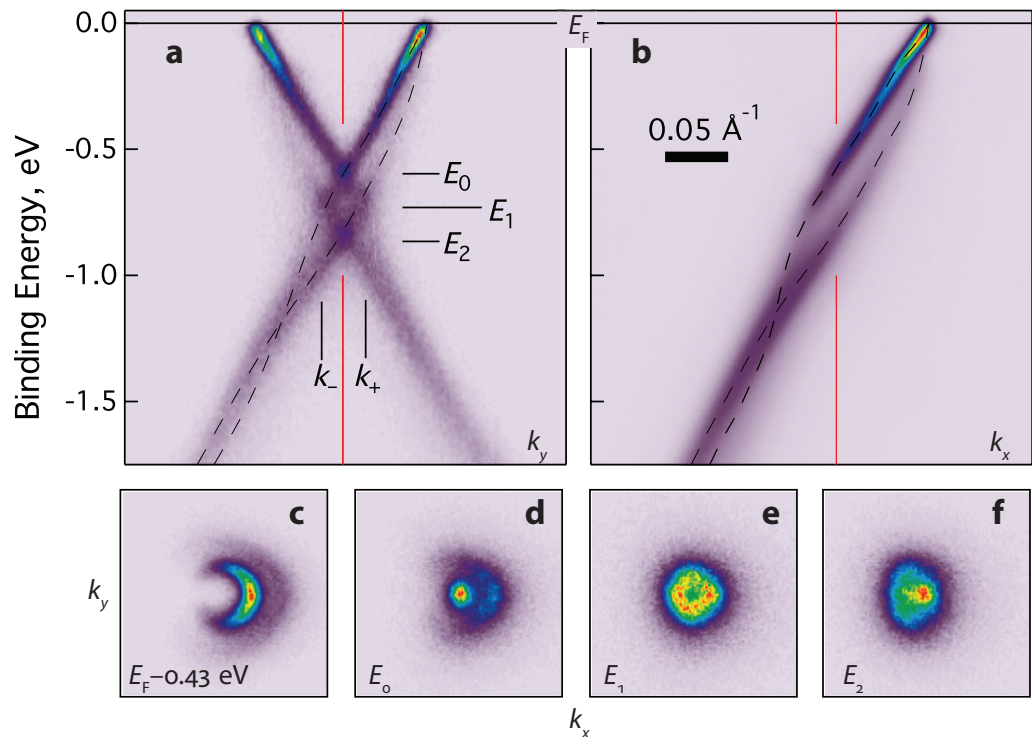
Figure 6. Slices of the ARPES spectral function for K-doped quasi-free-standing graphene. (a, b) Band structure acquired perpendicular and parallel to the ΓK line of the Brillouin zone, respectively. The red lines represent the K-point in momentum space. (c–f) Momentum distribution maps for the energy slices taken at energies $E_F = 0.43$ eV and E_{0-2} defined in panels (a, b). Adapted from [37].

composite particle, which was predicted as long ago as 1967 by Lundqvist for three-dimensional materials [39]–[41], and by von Allmen in two dimensions [42], and was named *plasmaron* by Lundqvist.

A detailed comparison of the experiment and theory convincingly demonstrates that this *plasmaronic* (to coin a term) quasi-particle explains the observed spectral function, and by extension, the spectral function of the ordinary graphene on SiC samples discussed earlier [37]. It remains only to explain why the earlier samples discussed in the first part of the paper displayed a much smaller splitting than the quasi-free-standing ones. This could be explained by the different interface between graphene and the substrate. In addition to screening within the graphene layer, it is expected that the nearby interface can provide additional screening to weaken the Coulomb interaction within the graphene. Theoretical considerations [30] show that this additional screening will greatly reduce the splitting between main and plasmaronic bands.

The role of hydrogen in the quasi-free-standing graphene samples (to be contrasted with its quite different role as an adsorbate on the graphene discussed in the next section) is to saturate the underlying Si dangling bonds in the substrate, which play a strong role at the ordinary SiC–graphene interface [26]. These dangling bonds when unsaturated are quite polarizable, and their removal from the quasi-free-standing samples leads to greatly reduced screening and hence the larger observed splitting.

The observation of the plasmaronic bands points to the deeper meaning of the ARPES measurements. Figure 7 shows a comparison between the (naively) expected and actually
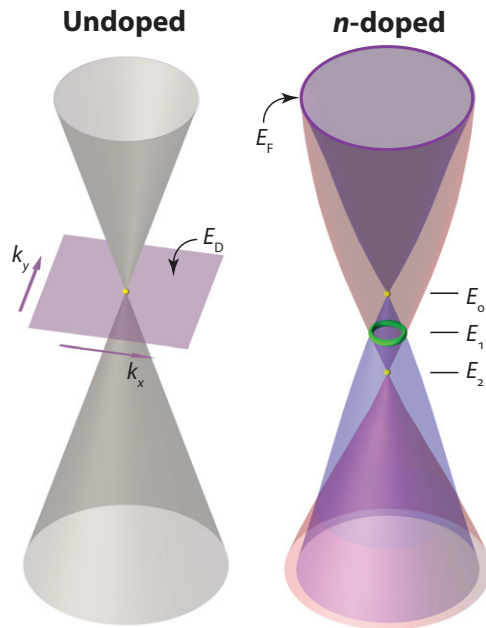
Figure 7. Conceptual illustration of the quasi-particle excitation spectrum for (left) undoped and (right) n-doped graphene (adapted from [37]).

observed quasi-particle spectra. The single linear conical bands in the former represent the states responsible for electronic conduction, but only in one of two limits: either in undoped graphene when $E_F \to E_D$ or in the weak interaction (or strong screening) limit. For doped quasi-free-standing graphene, as we have observed the spectrum is completely reconstructed. This reflects the fact that ARPES measures the final state of a system where one electron is removed, at which time the system internally reorganizes into multiple final states. Thus, ARPES measures the true excited-state spectrum, in which new propagating entities can be found.

The observation of such multiple propagating entities in ARPES is rare, but not unique. The separation of the single quasi-particle into charge and spin bands has been predicted and observed for one-dimensional cuprates [43, 44], for example.

3. Hydrogen on graphene

The validity of the quasi-particle picture for K-doped graphene is in dramatic contrast to the situation for atomic H interacting with graphene [9]. Figure 8 shows the Fermi surfaces and underlying band structures for clean and H-dosed graphene for various coverages of H. From these data, we make several important observations.

Observation 1. Although there is a strong reconstruction of the energy spectrum, there is always a Fermi surface. This means that whatever interpretation we choose for the remaining observations, an ordinary band insulator (as predicted for high coverages of hydrogen [45, 46] or for periodic arrangement of sparse H atoms [10]) is excluded by the data.

Observation 2. From the observed reduction in radius of the Fermi surface with H exposure, we conclude that hydrogen acts as a p-dopant. This is intuitively clear from the point of view of figure 1, where the saturation of a C p_z orbital should remove an electron from the graphene conduction band. If each H atom removes a single electron, then the H density n_H specified in figure 8 can be obtained directly from the reduction in the Fermi surface area. However, it
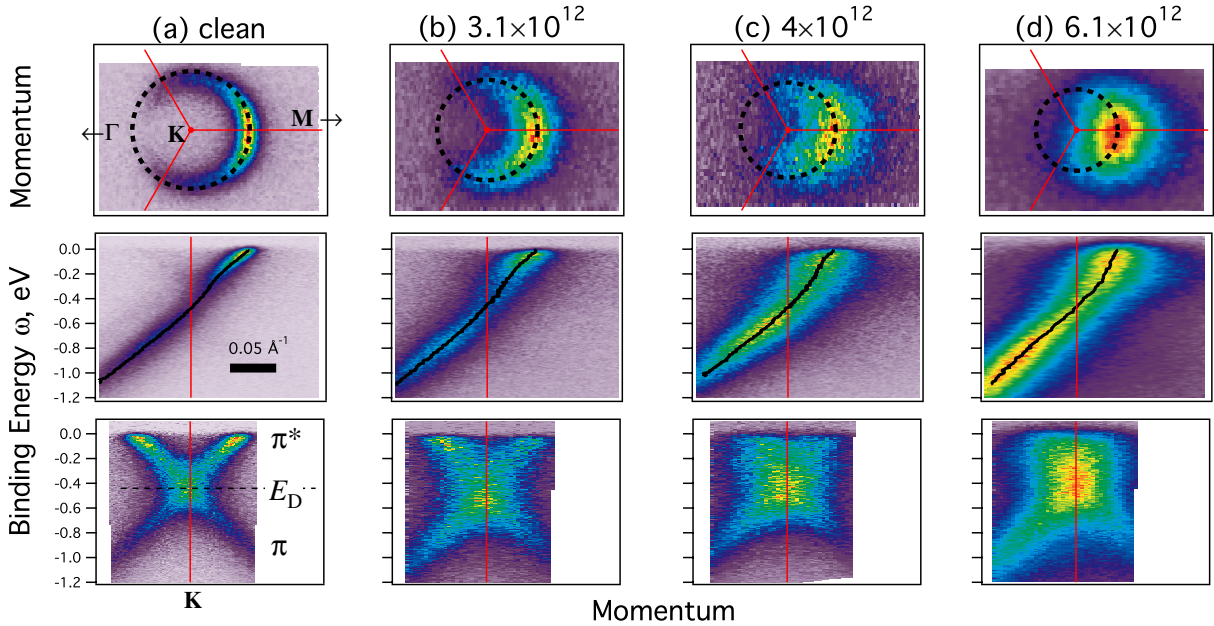
Figure 8. The Fermi surfaces (upper row) and band structure along two orthogonal directions (middle, bottom rows) for (a) clean and (b–d) progressively higher doses of atomic hydrogen, as indicated by the figure labels. A metal–insulator transition is observed between panels (b) and (c) (adapted from [9]).

should be noted that the observation of p-doping is in contradiction to calculations [47], which predict n-doping.

Observation 3. The kink in the bands at $\omega \sim 200\,\mathrm{meV}$ below E_F, described above as being due to electron–phonon coupling, can be observed at low H coverage, but disappears gradually at higher coverage and is gone at the highest coverage studied. This could be an indication that the lifetime of the electrons near E_F, previously long, is now shorter than the typical electron–phonon interaction time and so electron–phonon coupling cannot be observed.

Observation 4. There is a strong increase in the spectral linewidth of the Fermi surface with H coverage. Most significantly, at the highest coverage, the momentum width of the bands exceeds the radius of the Fermi surface k_F. This calls into question the validity of the quasi-particle picture for H/graphene, which is quite remarkable considering the low density of H atoms adsorbed (a few tenths of 1%).

Observation 5. There is an upward shift of spectral weight towards E_F. This leads at highest coverage to a gradual upturn of the upper, π^*, band. What is remarkable about this is the implication that the density of states $\mathcal{D}(\omega)$ near E_F is gradually reduced to zero. This can be evaluated numerically by the general form of $\mathcal{D}(\omega)$ for two dimensions,

$$\mathcal{D}(\omega) = \frac{2}{\pi} k(\omega)\, \mathrm{d}k(\omega)/\mathrm{d}\omega, \tag{2}$$

where $k(\omega)$ is the radius of the Fermi surface as a function of binding energy ω and the factor of 2 arises from the valley-degeneracy in graphene. The vanishing of $\mathcal{D}(\omega)$ near E_F is directly obtained from the vanishing slope of the band at high H concentration.

Observation 6. There is a notable asymmetry in the effects of H on the upper (π^*) and lower (π) bands. Whereas the slope of the upper band is heavily renormalized, the lower band

dispersion is rather unaffected, apart from an increase in its linewidth. Even with respect to linewidth, the effects on the lower band are not nearly as dramatic. While the upper band increases its linewidth by about a factor of 6 for the dosing range studied, the lower band broadens by only a factor of 2 for the same conditions. In contrast to the initial surface, where the quasi-particle linewidth increases as $\omega \to 0$, for H/graphene, the shortest lifetime is at E_F. This suggests not only a breakdown of the quasi-particle picture, but also a breakdown of the Fermi liquid picture.

Although not apparent in figure 8, where the data are plotted relative to the Fermi level E_F, we have made one additional crucial observation, that is, the overall band spectrum including the Fermi edge begins to shift to lower kinetic energy, starting at a critical hydrogen coverage $n_H \sim 3 \times 10^{12} \, \mathrm{cm}^{-2}$ and shifting further with continued dosing. This is an indication of charging of the sample and leads to the following.

Observation 7. There is metal–insulator transition at a critical hydrogen coverage. Whereas for pristine samples the resistance R is extremely low (the samples can sustain electrical currents of about 400 mA without noticeable warming), above the critical H coverage the sample quickly reaches a resistance R of about $10 \, \mathrm{M\Omega}$. This can be determined from $R = V/I$, where V is the observed kinetic energy shift and I the measured photocurrent.

This determination of R is possible because of two factors: firstly, the measurement was made with one side of the sample floating, so that the path of the photocurrent through the sample was directed from one sample clip to the photon beam, and secondly, because the photon spot diameter (50 μm) was much smaller than the size of the sample. By this means, the resistance measurement was straightforward. By comparing the resistance measured at different points on the sample, we could determine unambiguously that the resistance arose in the sample, and not at the interface between the sample and the clip, or through to the substrate, for example. (Differential measurement of the resistance at two neighbouring points is equivalent to a four-probe resistance measurement, with the advantage of being free of physical contacts to the sample.)

The observation of an intact Fermi surface on both sides of the metal–insulator transition is strong evidence that the observed resistance arises not from the development of an insulating band structure, but instead strong quantum-mechanical corrections to the conductivity. In particular, the breakdown of the quasi-particle picture (i.e. when the width of the states in momentum space is larger than the Fermi wavelength k_F) in conjunction with the appearance of resistance suggests that at a critical coverage, atomic H induces a strong localization regime (i.e. Anderson localization [48]). Put simply, the quasi-particle picture breaks down because localized states are not quasi-particles. In this view, across the MIT, the interpretation of the ARPES spectrum in terms of a single-particle spectral function equation (1) becomes invalid, and instead the momentum spread of the states becomes in some sense a measure of the localization length.

Such localization effects have been predicted theoretically from symmetry considerations [12, 13] and by tight-binding simulations [49, 50] and experiments on carbon nanotubes [51] for defect densities similar to our experiments. The work [37] represented the first strong experimental evidence for Anderson localization in graphene.

More recently, additional evidence has been presented for such strong localization in graphene. The observed spectral functions in figure 8 have been successfully simulated [52], substantially confirming the interpretation of the ARPES data in terms of strong localization. More recently, Anderson localization was also confirmed by magnetotransport measurements of ozone-damaged graphene [53] at similar defect densities.

The observed preferential reconstruction of the π^* density of states and other asymmetries with respect to the Dirac crossing energy E_D is consistent with a predominant scattering from an H-induced resonant state consistent with predictions. Unlike K atoms, which are long-range Coulomb scatterers and induce weak antilocalization, H atoms are short range and induce weak localization [12, 13]. Weak localization is a precursor of Anderson localization, in which the backscattering amplitude from short-range scatterers in the presence of wave coherence causes the absence of conductance [48]. Ioffe and Regel [54] and Mott [55] suggested that strong localization occurs when the mean free path l_{mfp} becomes smaller than the inverse Fermi wavevector k_F^{-1}. Our data show that localization sets in earlier, at $l_{mfp}k_F \sim \frac{1}{2}$.

Anderson localization is very dramatically manifested here because of the exceptionally large cross section for scattering by H atoms, the very long Fermi wavelength of graphene and the epitaxial bonding of graphene to the substrate, which keeps the distortion of the lattice by H atoms extremely short range, while the interstitial graphene remains a pristine massless Dirac metal. This is in contrast to exfoliated flakes on SiO_2, where waves in the graphene due to substrate roughness and intrinsic rippling have been shown to weaken (anti-) localization in the low-disorder regime [56, 57].

Our results also put earlier photoemission measurements in a new perspective. The spectra in figure 8(b) are practically identical to those of incomplete graphene layers comprised of small islands [58, 59], also showing a split energy spectrum at the K point, reduced Fermi surface area and broadening. Since such samples were formed without hydrogen present, we can infer that these spectral features are generic to certain lattice defects and not symmetry-breaking due to either substrate interactions, as proposed in [25, 26], or the formation of band insulators such as graphane [45, 46]. It also suggests that the spectral features we observe are a generic feature of a class of defects and not unique to hydrogen.

In summary, we have shown that many-body interactions are profoundly important for understanding the ARPES spectral function of both atomic-K- and atomic-H-dosed graphene samples, although these two adsorbates induce completely different dynamical regimes. In the former, the quasi-particle lifetime remains long, and the system is protected from localization by the long-range nature of the defects introduced by the dopants. By removing the screening influence of the substrate, we showed the presence of multiple quasi-particles, which can be well described by the standard many-body interpretation of ARPES. In the case of H adsorption, the quasi-particle picture is spectacularly violated, and the ARPES spectrum can be interpreted as a measure of the localization lengths due to defect scattering. The prospect for future measurements of the localized system is particularly interesting because until now there has not been a clear demonstration of such localization by direct surface probe, such as scanning tunnelling microscopy. Such measurements would be very interesting to study unresolved questions about the Anderson transition, such as its occurrence in confined structures.

References

[1] DiVincenzo D P and Mele E J 1984 Self-consistent effective-mass theory for intralayer screening in graphite intercalation compounds *Phys. Rev.* B **29** 1685–94

[2] Ando T and Nakanishi T 1998 Impurity scattering in carbon nanotubes—absence of back scattering *J. Phys. Soc. Japan* **67** 1704–13

[3] Ando T, Nakanishi T and Saito R 1998 Berry's phase and absence of back scattering in carbon nanotubes *J. Phys. Soc. Japan* **67** 2857–62

[4] Novoselov K S, McCann E, Morosov S V, Fal'ko V I, Katsnelson M I, Zeitler U, Jiang D, Schedin F and Geim A K 2005 Two-dimensional gas of massless Dirac fermions in graphene *Nature* **438** 192–200

[5] Zhang Y, Tan Y W, Stormer H L and Kim P 2005 Experimental observation of the quantum Hall effect and Berry's phase in graphene *Nature* **438** 201–4

[6] Ohta T, Bostwick A, Seyller T, Horn K and Rotenberg E 2006 Controlling the electronic structure of bilayer graphene *Science* **313** 951–4

[7] Bostwick A, Ohta T, Seyller T, Horn K and Rotenberg E 2007 Quasiparticle dynamics in graphene *Nat. Phys.* **3** 36–40

[8] Ohta T, Bostwick A, McChesney J L, Seyller T, Horn K and Rotenberg E 2007 Interlayer interaction and electronic screening in multilayer graphene investigated with angle-resolved photoemission spectroscopy *Phys. Rev. Lett.* **98** 206802

[9] Bostwick A, McChesney J L, Emtsev K V, Seyller T, Horn K, Kevan S D and Rotenberg E 2009 Quasiparticle transformation during a metal insulator transition in graphene *Phys. Rev. Lett.* **103** 056404

[10] Duplock E J, Scheffler M and Philip Lindan J D 2004 Hallmark of perfect graphene *Phys. Rev. Lett.* **92** 225502

[11] Koike Y, Suematsu H, Higuchi K and Tanuma S 1978 Superconductivity in graphite–potassium intercalation compound C8K *Solid State Commun.* **27** 623–7

[12] Suzuura H and Ando T 2002 Anderson localization in a graphene sheet *J. Phys. Soc. Jpn.* **72** (Suppl. A) 69–70

[13] Suzuura H and Ando T 2002 Crossover from symplectic to orthogonal class in a two-dimensional honeycomb lattice *Phys. Rev. Lett.* **89** 266603

[14] Aleiner I L and Efetov K B 2006 Effect of disorder on transport in graphene *Phys. Rev. Lett.* **97** 236801–4

[15] Bennich P, Puglia C, Brhwiler P A, Nilsson A, Maxwell A J, Sandell A, Martensson N and Rudolf P 1999 Photoemission study of K on graphite *Phys. Rev.* B **59** 8292–304

[16] Jeloaica L and Sidis V 1999 DFT investigation of the adsorption of atomic hydrogen on a cluster-model graphite surface *Chem. Phys. Lett.* **300** 157–62

[17] Forbeaux I, Themlin J M and Debever J M 1998 Heteroepitaxial graphite on 6H-SiC(0001): interface formation through conduction-band electronic structure *Phys. Rev.* B **58** 16396–406

[18] Emtsev K V, Seyller T, Speck F, Ley L, Stojanov P, Riley J D and Leckey R G C 2006 Initial stages of the graphite–SiC(0001) interface formation studied by photoelectron spectroscopy arXiv:cond-mat/0609383

[19] Emtsev K V, Speck F, Seyller T, Ley L and Riley J D 2008 Interaction, growth, and ordering of epitaxial graphene on SiC0001 surfaces: a comparative photoelectron spectroscopy study *Phys. Rev.* B **77** 155303–10

[20] Damascelli A, Hussain Z and Shen Z X 2003 Angle-resolved photoemission studies of the cuprate superconductors *Rev. Mod. Phys.* **75** 473

[21] Kaminski A and Fretwell H M 2005 On the extraction of the self-energy from angle-resolved photoemission spectroscopy *New J. Phys.* **7** 98

[22] Shirley E L, Terminello L J, Santoni A and Himpsel F J 1995 Brillouin-zone-selection effects in graphite photoelectron angular distributions *Phys. Rev.* B **51** 13614–22

[23] Bostwick A, Ohta T, McChesney J L, Emtsev K V, Seyller T, Horn K and Rotenberg E 2007 Symmetry breaking in few layer graphene films *New J. Phys.* **9** 385

[24] Mucha-Kruczynski M, Tsyplyatyev O, Grishin A, McCann E, Fal'ko V I, Bostwick A and Rotenberg E 2008 Characterization of graphene through anisotropy of constant-energy maps in angle-resolved photoemission *Phys. Rev.* B **77** 195403

[25] Zhou S Y, Gweon G H, Fedorov A V, First P N, de Heer W A, Lee D H, Guinea F, Castro A H Neto and Lanzara A 2007 Substrate-induced bandgap opening in epitaxial graphene *Nat. Mater.* **6** 770–5

[26] Kim S, Ihm J, Choi H J and Son Y-W 2008 Origin of anomalous electronic structures of epitaxial graphene on silicon carbide *Phys. Rev. Lett.* **100** 176802–4

[27] Park C-H, Giustino F, Cohen M L and Louie S G 2007 Velocity renormalization and carrier lifetime in graphene from the electron–phonon interaction *Phys. Rev. Lett.* **99** 086804–4

[28] Tse W-K and Sarma S D 2007 Phonon-induced many-body renormalization of the electronic properties of graphene *Phys. Rev. Lett.* **99** 236802–4

IOP Institute of Physics ⊕ DEUTSCHE PHYSIKALISCHE GESELLSCHAFT

[29] Hwang E H and Das Sarma S 2007 Dielectric function, screening, and plasmons in two-dimensional graphene *Phys. Rev.* B **75** 205418

[30] Polini M, Asgari R, Borghi G, Barlas Y, Pereg-Barnea T and MacDonald A H 2008 Plasmons and the spectral function of graphene *Phys. Rev.* B **77** 081411–4

[31] Hwang E H and Sarma S D 2008 Quasiparticle spectral function in doped graphene: electron–electron interaction effects in ARPES *Phys. Rev.* B **77** 081412–4

[32] Park C-H, Giustino F, Spataru C D, Cohen M L and Louie S G 2009 Angle-resolved photoemission spectra of graphene from first-principles calculations *Nano. Lett.* **9** 4234–9

[33] Benfatto L and Cappelluti E 2008 Spectroscopic signatures of massless gap opening in graphene *Phys. Rev.* B **78** 115434–5

[34] Skrypnyk Y V and Loktev V M 2008 Spectral function of graphene with short-range impurity centers *Low Temp. Phys.* **34** 818–25

[35] Riedl C, Coletti C, Iwasaki T, Zakharov A A and Starke U 2009 Quasi-free standing epitaxial graphene on SiC by hydrogen intercalation *Phys. Rev. Lett.* **103** 246804–8

[36] Speck F, Ostler M, Röhrl J, Jobst J, Waldmann D, Hundhausen M, Ley L, Weber H B and Seyller T 2010 Quasi-freestanding graphene on SiC(0001) *Mater. Sci. Forum* **645** 629–32

[37] Bostwick A, Speck F, Seyller T, Horn K, Polini M, Asgari R, MacDonald A H and Rotenberg E 2010 Observation of plasmarons in quasi-free-standing doped graphene *Science* **328** 999–1002

[38] Bohm D and Pines D 1953 A collective description of electron interactions: III. Coulomb interactions in a degenerate electron gas *Phys. Rev.* **92** 609

[39] Lundqvist B 1967 Single-particle spectrum of the degenerate electron gas. I. The structure of the spectral weight function *Phys. Kondens. Mater.* **6** 193–205

[40] Lundqvist B 1967 Single-particle spectrum of the degenerate electron gas. II. Numerical results for electrons coupled to plasmons *Phys. Kondens. Mater.* **6** 206–17

[41] Lundqvist B I 1968 Single-particle spectrum of the degenerate electron gas. III. Numerical results in the random phase approximation *Phys. Kondens. Mater.* **7** 117–23

[42] von Allmen P 1992 Plasmaron excitation and band renormalization in a two-dimensional electron gas *Phys. Rev.* B **46** 13345

[43] Kim C, Matsuura A Y, Shen Z X, Motoyama N, Eisaki H, Uchida S, Tohyama T and Maekawa S 1996 Observation of spin–charge separation in one-dimensional $SrCuO_2$ *Phys. Rev. Lett.* **77** 4054

[44] Kim J S, Boeri L, Kremer R K and Razavi F S 2006 Effect of pressure on superconducting Ca-intercalated graphite CaC6 *Phys. Rev.* B **74** 214513–6

[45] Sofo J O, Chaudhari A S and Barber G D 2007 Graphane: a two-dimensional hydrocarbon *Phys. Rev.* B **75** 153401–4

[46] Elias D C *et al* 2009 Control of graphene's properties by reversible hydrogenation *Science* **323** 610–3

[47] Boukhvalov D W, Katsnelson M I and Lichtenstein A I 2008 Hydrogen on graphene: electronic structure, total energy, structural distortions and magnetism from first-principles calculations *Phys. Rev.* B **77** 035427–7

[48] Anderson P W 1958 Absence of diffusion in certain random lattices *Phys. Rev.* **109** 1492

[49] Naumis G G 2007 Internal mobility edge in doped graphene: frustration in a renormalized lattice *Phys. Rev.* B **76** 153403–4

[50] Amini M, Jafari S A and Shahbazi F 2009 Anderson transition in disordered graphene *Euro. Phys. Lett.* **87** 37002 1–5

[51] Gomez-Navarro C, De Pablo P J, Gomez-Herrero J, Biel B, Garcia-Vidal F J, Rubio A and Flores F 2005 Tuning the conductance of single-walled carbon nanotubes by ion irradiation in the Anderson localization regime *Nat. Mater.* **4** 534–9

[52] Skrypnyk Y V and Loktev V M 2010 Metal–insulator transition in hydrogenated graphene as manifestation of quasiparticle spectrum rearrangement of anomalous type arXiv:1008.2559 [cond-mat]

[53] Moser J, Tao H, Roche S, Alzina F, Sotomayor C M Torres and Bachtold A 2010 Magnetotransport in disordered graphene exposed to ozone: from weak to strong localization *Phys. Rev.* B **81** 205445

[54] Ioffe A F and Regel A R 1960 Non-crystalline, amorphous and liquid electronic semiconductors *Prog. Semicond.* **4** 237

[55] Mott N F 1967 Electrons in disordered structures *Adv. Phys.* **16** 49–144

[56] Morozov S V, Novoselov K S, Katsnelson M I, Schedin F, Ponomarenko L A, Jiang D and Geim A K 2006 Strong suppression of weak localization in graphene *Phys. Rev. Lett.* **97** 016801–4

[57] Morpurgo A F and Guinea F 2006 Intervalley scattering, long-range disorder, and effective time-reversal symmetry breaking in graphene *Phys. Rev. Lett.* **97** 196804–4

[58] Rotenberg E, Bostwick A, Ohta T, McChesney J L, Seyller T and Horn K 2008 Origin of the energy bandgap in epitaxial graphene *Nat. Mater.* **7** 258–9

[59] Zhou S Y, Siegel D A, Federov A V, Gabaly F E, Schmid A K, Castro Neto A H, Lee D H and Lanzara A 2008 Origin of the energy bandgap in epitaxial graphene [reply] *Nat. Mater.* **7** 259–60